



Universiteit Utrecht

BACHELOR THESIS

**Performance study for the D^{*+}
reconstruction using the ALICE ITS
upgrade**

Author:

Jonathan DE JAGER

Student number: 4166647

Study: Physics & Astronomy

Supervisors:

Dr. André MISCHKE

Utrecht University

and

Dr. Alessandro GRELLI

Utrecht University

15 June 2016

Abstract

According to calculation of Quantum Chromodynamics on the lattice, a phase transition to a Quark-Gluon Plasma occurs under the conditions of high energy density and temperature. These conditions are reached in the ALICE experiment with high-energy collisions of lead nuclei. The ALICE detectors, including the Inner Tracking System, will be upgraded in 2019 – 2020. This research project studied D^{*+} reconstruction with the upgraded ITS. To study the performance, the improvement of detecting D^{*+} mesons with low p_t and the expected significance of D^{*+} mesons for p-p collisions as well as for Pb-Pb collisions is investigated. For both subjects a Monte-Carlo simulation program PYTHIA is used to generate high-energy collision events. To study the acceptance of D^{*+} mesons with a low p_t , a minimum p_t of 40 MeV/c is used for the soft pion. To calculate the significance, real data is used for estimating the background. The data to calculate the background is produced in p-p collision at $\sqrt{s_{NN}} = 13$ TeV and Pb-Pb collisions at $\sqrt{s_{NN}} = 2.76$ TeV.

58% of the D^{*+} mesons with a p_t between the 0 and 0.5 GeV/c can be reconstructed, and 90 % or more for D^{*+} mesons with a p_t higher than 0.5 GeV/c. The significance is calculated higher than 5 in all p_t ranges up to 36 GeV/c, except for D^{*+} mesons with a p_t lower than 0.5 GeV/c produced in Pb-Pb collisions.

Contents

1	Introduction	1
2	Theoretical Framework	3
2.1	Standard Model	3
2.2	Quantum chromodynamics	4
2.3	Quark-gluon plasma	4
2.4	D*mesons	6
3	Experimental Setup	7
3.1	ALICE detectors	7
3.1.1	Inner Tracking System	7
3.1.2	Time projection chamber	8
3.1.3	Time of Flight detector	8
3.2	Analysis method	10
3.2.1	Simulation program PYTHIA	10
3.2.2	ROOT	10
4	Analysis	11
4.1	Simulation	11
4.1.1	Configuration	11
4.1.2	Comparison heavy flavour forced and minimum bias simulation	11
4.1.3	General characteristics D* meson production	12
4.2	Real data	16
4.2.1	Invariant Mass method	17
4.2.2	Performed cuts	17
5	Results p_t-range	19
6	Results significance D*	22
6.1	Expected yield	22
6.2	Background	23
6.3	Expected significance	23
7	Discussion	28
8	Conclusion & Outlook	29
8.1	Conclusion	29
8.2	Outlook	29
	Appendix A	I

Chapter 1

Introduction

Approximately a microsecond after the big bang, the universe was so hot and dense it is expected that a phase of matter existed, called a quark-gluon plasma (QGP). In this phase, quarks and gluons form a plasma, and are not confined in particles like protons, neutrons, or in this study, D^{*+} mesons. It is predicted that this phase can also be created in a particle accelerator. When two particles are collided, there is not enough energy available to produce this plasma. However, when multiple particles collide at the same time, enough energy is available for a phase transition to a quark-gluon plasma.

In the Large Hadron Collider (LHC), lead nuclei collide with enough energy to produce the quark-gluon plasma. The plasma is investigated by an experiment called ALICE (A Large Ion Collider Experiment). To investigate the plasma, ALICE uses particle detectors which are specifically designed to measure particles coming from collisions between lead (Pb) ions. The detector closest to the point where the collisions take place is called the Inner Tracking System (ITS). Due to the fact that the ITS is placed close to the high energy collisions, the performance of the detector decreases over time. Because of this effect the detector has to be replaced in 2019-2020. When the ITS is replaced in 2019-2020, it will also get an upgrade. Not only will the new ITS consist of seven layers instead of six, all detectors will be replaced with pixes-detectors which have a higher resolution. In this research project can be investigated what to be expected after the upgrade.

In this project, the performance of the ITS is investigated for reconstructing the D^{*+} meson. The D^{*+} meson turns out to be a good probe to study the quark-gluon plasma. Because the quark-gluon plasma is produced in Pb-Pb collisions and not in p-p collisions, both collisions are measured. The D^{*+} mesons produced in p-p collisions will be a reference for D^{*+} mesons produced in Pb-Pb collisions. The difference between these two collisions give us information about the plasma. The D^{*+} meson, however, cannot be detected directly. It will decay twice before reaching the detector. There are a lot of different decay-modes in which the D^{*+} meson can decay. The focus of this thesis will be on the decay-mode where the D^{*+} meson decays into a D^0 and a π^+ . This D^0 again decays into a K^- and a π^+ . Other decays will be shortly discussed but the final results are obtained by studying these decays.

As discussed in the previous paragraph, the aim of this research project is to study the performance of the ALICE ITS detector for reconstructing D^{*+} mesons after the upgrade in 2019-2020. The performance is studied on the basis of what percentage of the D^{*+} particles with a low p_t can be detected, and what the expected significance is of D^{*+} particles produced in p-p collisions and Pb-Pb collisions. To investigate the percentage of D^{*+} mesons with a low p_t a simulation is used. To calculate the significance both simulation and real data are used. The simulation is used to calculate the expected yield and real data taken from ALICE is used to calculate the background. The yield and the background will be combined to calculate the significance.

In the first chapter a theoretical background is given for the Standard Model, quantum chromodynamics and the quark-gluon plasma. At the end of this chapter some characteristics of the D^{*+} meson are discussed. In the part where theoretical background is

given for the quark-gluon plasma, it is discussed why the D^{*+} meson is a good probe to investigate the plasma. In the second chapter an overview is given of the main detectors used by ALICE. For every detector will be discussed shortly what will change after the upgrade. The software used for analysis are described shortly at the end of the second chapter. In the third chapter the analysis are presented for both the simulation and the real data. The following chapters contain the results for both the significance and the investigation of low $p_t D^{*+}$ mesons. In chapter 7 the presented results are discussed and a conclusion is drawn. The thesis ends with a short outlook where possible further study is discussed.

Chapter 2

Theoretical Framework

2.1 Standard Model

The Standard Model is currently the most general theory for particle physics. The Standard Model classifies all known subatomic particles and describes the electromagnetic, weak and strong force. The confirmed existence of the Higgs boson in 2010, which was predicted by this theory, was the missing piece that was found. Although the Standard Model is very successful in explaining almost all experimental results, it does not include the gravitation described by the theory of general relativity. A schematic overview of the Standard Model is given in fig 2.1. The model divides the fundamental particles in three different parts. The particles with a spin $=\frac{1}{2}$ are called fermions. Particles with spin $= 1$ are called Gauge Bosons, while the Higgs particles have a spin of 0.

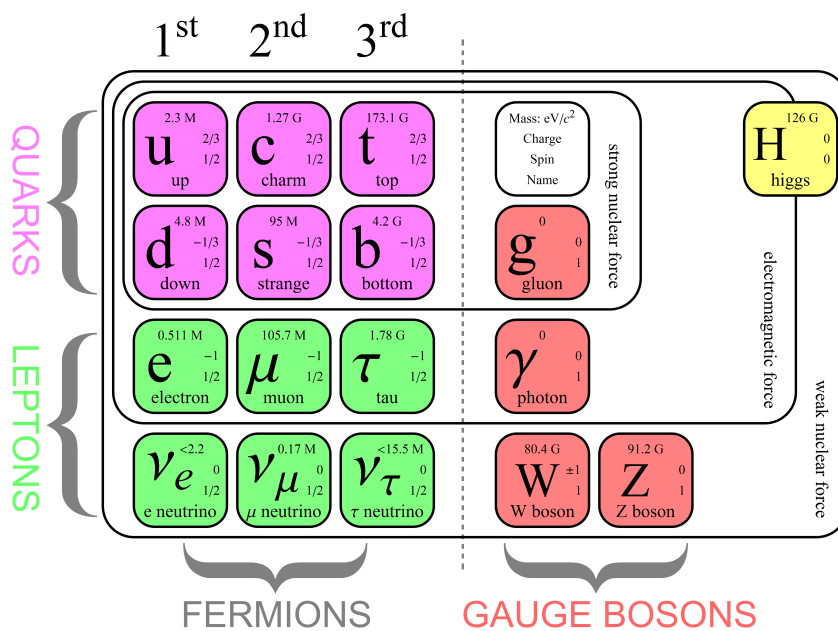


Figure 2.1 – Schematic overview of the Standard Model[2].

The Fermions are divided in Leptons and Quarks. There are three generations of Fermions, where the first generation is formed by the up (u) and down (d) quark, next to the electron (e) and the electron neutrino (ν_e) as leptons. The first generation particles are the stable particles. These particles are the building blocks of matter. The second generation fermions consists of the charm (c) and the strange (s) quark, next to the muon (μ) and its neutrino (ν_μ) as leptons. The third generation consists of a top and bottom quark, next to a tau and its neutrino as described in figure 2.1. Second and third generation particles can be produced in a particle accelerator when sufficient energy is

available. However, this second and third generation particles are not stable and will therefore decay in lower generation particles after a short lifetime.

Gauge bosons are force carriers. There are three different forces which are carried by 4 Gauge bosons: the electromagnetic force, the weak force and the strong force. The electromagnetic force between charged particles is carried by a photon. This means that when two charged particles interact, the interaction is carried from one charged particle to the other by a photon. The weak force is mediated by the W^+ , W^- and the Z boson, while the strong force is carried by gluons.

The electromagnetic force is described by the quantum electrodynamics (QED). Together with the weak force these two forces can be combined to the electroweak interaction. The weak force is applicable to all fermions but is, as its name suggests, significant weaker than the strong and the electromagnetic force. The strong force is only applicable to quarks and dominates at small distances. The strong interaction is described by quantum chromodynamics (QCD).

2.2 Quantum chromodynamics

Quantum chromodynamics describes the strong interaction between quarks and gluons. Where QED describes the electromagnetic interaction between particles with charge, QCD describes the strong interaction between particles with a color charge. Both quarks and gluons carry color charge. There are three different color charges: red, green and blue. For each color exists an anti-color charge: anti-red, anti-green and anti-blue. This quantum number has no physical connection with visible colors except that red, blue and green together become white or colorless. *Colorless* means as much as *neutral* means in electromagnetic charge. Besides containing the combination of all colors, a particle also becomes colorless when carrying both a color and its anti-color. Because quarks are always observed together in bound states, all observable particles are colorless,. These particles are called hadrons. Hadrons can be divided in two groups. A particle containing two quarks is called a meson and a particle with three quarks is called a baryon. Mesons always consist of a quark and an anti-quark. The quark and the anti-quark have such a color and an anti-color that the particle is colorless. Baryons always consist of three quarks, all with a different color. QCD described two other phenomena: confinement and asymptotic freedom. Confinement means that the force between quarks does in fact increase when two quarks are separated. When quarks are separated, the energy of the gluon field becomes so high that a quark anti-quark pair can be created. This quark pair will form a meson together. If enough energy is available, many hadrons can be produced by separating two quarks. The stream of particles which are produced by separating quarks is called a jet. This phenomenon is not analytically proven, but explains well the fact that single quarks are never observed. Asymptotic freedom is a feature of QCD and means that the strong interaction between quarks and gluons gets weaker when energy gets higher or the distance between particles closer. This effect is believed to be caused by antiscreening. Antiscreening is the opposite of screening in QED. In QED, virtual pairs of electrons and positrons in the vicinity of a charged particle polarize the vacuum. For example, when the charged particle has a positive charge, the electrons will be attracted to the particle and the positrons will be pulled away. This will diminish the electrical field at larger distances. In QCD this phenomena is comparable with QED. Instead of diminishing the field, virtual gluons will enhance the net color of the particle. Therefore, when two quarks are close, fewer virtual pairs of gluons will be between the quarks and the force between the quarks will be lower. Quarks which are confined are therefore asymptotically free within the dimensions of a particle.

2.3 Quark-gluon plasma

Asymptotic freedom also occurs at very high energies or densities. Quarks and gluons are predicted to form a quark-gluon plasma (QGP) when reaching these extreme values. The volume in which quarks are asymptotical free is much larger in a QGP than asymptotical

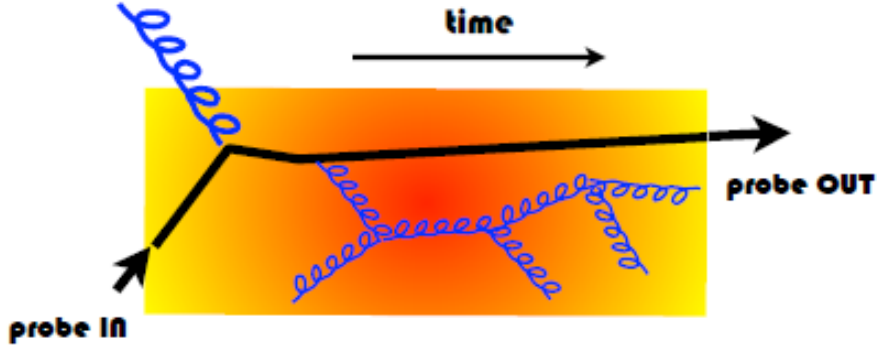


Figure 2.3 – Schematic overview of a probe entering the quark-gluon plasma, emitting gluons and leaving the plasma [4].

is suppressed by what is called the dead cone effect. This effect suppresses the radiation under a certain angle $\theta = \frac{m_q}{E_q}$. The angle is proportional to the mass of the quark. This means the heavier the quark, the less energy it loses by radiating gluons, and the better the interaction of quarks with the plasma can be investigated.

To compare the energy loss of quarks, the results of collisions between lead ions are compared with results of collisions between protons. The factor used to compare these results is the nuclear modification factor R_{AA} . R_{AA} is the yield produced in proton collisions divided by the yield produced in lead collisions and normalized for the number of particles created. The nuclear modification factor is defined as following:

$$R_{AA}(p_t) = \frac{dN_{AA}/dp_t}{\langle T_{AA} \rangle * d\sigma_{pp}/dp_t}. \quad (2.3.1)$$

Where AA stands for the heavy ions that are collided (in ALICE this would be PbPb). The term dN_{AA}/dp_t is the yield by lead collisions and $d\sigma_{pp}/dp_t$ is the yield proton collisions. $\langle T_{AA} \rangle$ is the nuclear overlap function which takes into account the fact that more nucleons collide at the same time when colliding lead ions. The factor would be one if there is no plasma created by heavy ion collisions.

2.4 D*mesons

As discussed in the previous section, probes to investigate the QGP should have a high energy in order to have a small production time and to lose less energy by radiating gluons. However, particles with a high mass are produced more rarely than light particles. To have enough statistics but high enough mass to be certain that the probe is produced before the QGP the D^{*+} meson is often used as a probe to investigate the QGP. The D^{*+} particle is a meson and consists of two quarks. Just as the D^+ the D^{*+} has a $c\bar{d}$ quark pair. The D^{*+} is therefore an excited state of the D^+ . The D^{*+} can be produced when a charm and a anti-down quark form a particle together or when a D^{*+} is a decay product of another particle. This can be an higher excited D- meson like the $D_1(2420)^0$ or a B-meson. When a D^{*+} is produced it can decay following three decay modes[5]:

$$\begin{aligned} D^{*+} &\rightarrow D^0 + \pi^+ && (67.7\% \pm 0.5) \\ D^{*+} &\rightarrow D^+ + \pi^0 && (30.7\% \pm 0.5) \\ D^{*+} &\rightarrow D^+ + \gamma && (1.6\% \pm 0.4) \end{aligned}$$

In this research project the decay mode $D^{*+} \rightarrow D^0 + \pi^+ \rightarrow \kappa^- + 2\pi^+$ will be investigated. No distinction will be made between a particle and its anti-particle. Therefore the D^{*+} and the D^{*-} will be called D*.

Chapter 3

Experimental Setup

3.1 ALICE detectors

ALICE (A Large Ion Collider Experiment) is one of the four particle detectors at the Large Hadron Collider at CERN. It is designed to study heavy ion collisions with high enough energy to form a QGP. ALICE consists of multiple detectors which can be divided into two groups. The first group consists of detectors, which are located perpendicular to the collision beam at the location of the collision point. The goal of these detectors is to measure hadronic particles. The other group of detectors is placed more alongside the collision beam. These detectors measure mainly muons and is used for triggers. In this thesis, primarily the first part of the detectors is used. The most important detectors will be discussed in the following paragraphs.

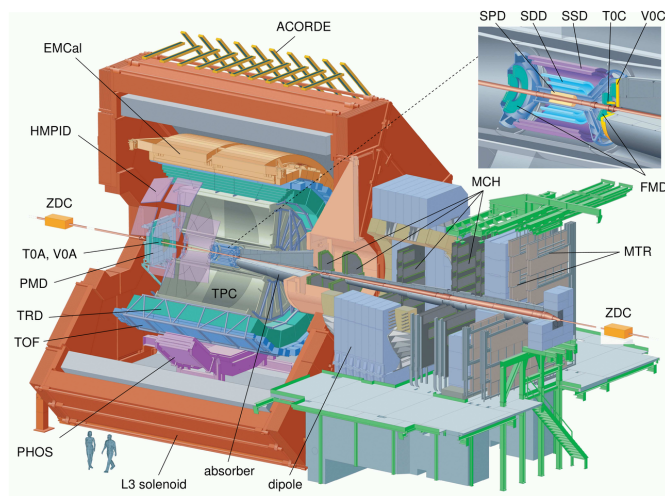


Figure 3.1 – Schematic overview of the ALICE detector at the CERN LHC.[6]

3.1.1 Inner Tracking System

The Inner Tracking System is the detector which detects particles first when produced. The ITS is closest to the collision point and has the following 3 functions[9]:

- determination of the position of the collision point and decay points,
- identifying and tracking low momentum particles,
- improvement of the momentum and angle measurements of the TPC.

The ITS consists of 6 layers of silicon detectors. The closest layer has a radius of 3.9 cm and is a silicon pixel detector (SPD). SPD's have the highest resolution to determine

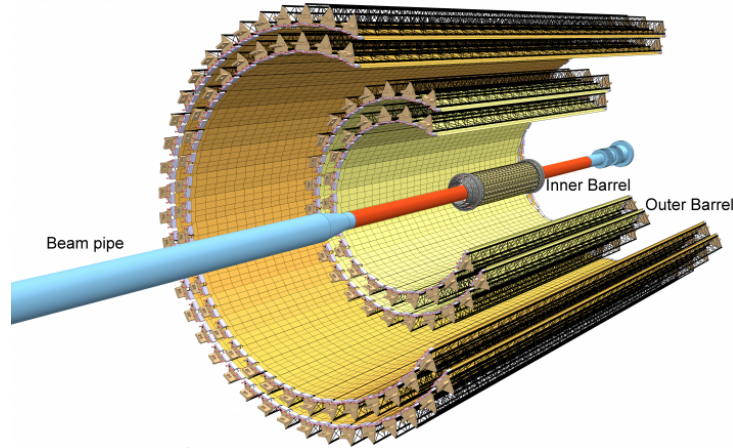


Figure 3.2 – Schematic overview of the ITS detector after the upgrade in 2019-2020.[7]

the place of a particle. The second layer is also an SPD and has a radius of 7.6 cm. The first and the fourth layer are both silicon drift detectors. SDD detectors have a lower resolution than SPD's and are placed at 15 and 23.9 cm from the collision point. The last two layers are placed at 38 and 43 cm and are silicon strip detectors[8]. These detectors, build at Utrecht University, have a great role in matching tracks between the ITS and the TPC. However with the upgrade in 2019 -2020 the ITS will consist of 7 layers of silicon detectors. The closest layer will have a radius of 2.2 cm and all layers will consist of the SPDs. The shorter distance between the first layer of the ITS and the collision point will result in the fact that particles with lower transverse momenta can also be detected. The result of the fact that all layer will have SPD's will mainly result in a better overall resolution.

3.1.2 Time projection chamber

The Time projection chamber(TPC) is the main tracking system of ALICE and consists of 2 chambers (shown in figure 3.3).The detector is 85 cm to 250 cm in the radial direction and 5 m long[14].The placement of the TPC is around the ITS. It is filled with a gas mixture of $Ne-CO_2-N_2$. After particles travel through the ITS they enter the TPC. In the TPC the particles will ionize the gas by knocking off electrons of gas molecules. The electric field will attract the gas-ions and the electrons to the end of the TPC where they can be detected. From the time it takes for electrons to reach the end of the chamber can be constructed what the position was in the beam direction. This conversion gives the TPC its name. The charge of the particle can be measured by the shape of the path. Positive particles are bend in the opposite direction of negative charged particles due to the magnetic field. For the best resolution, the mixture of the gas is calibrated with a ratio of 85.7% Ne – 9.5% CO_2 –4.8% N_2 [12]. The magnetic field is 0.5 T and homogeneous. The electric field is 400 V/cm[13]. In the upgrade, the detectors are upgraded to improve the read-out speed and resolution[11].

The main function of the TPC is to provide track finding, charged particle momentum measurement, particle identification, and two track separation in the region of $p_T < 10$ GeV. In figure 3.4 is an example of particle identification from energy loss of different particles.

3.1.3 Time of Flight detector

The Time of Flight (TOF) detector consists of a stack of 6 resistive glass plates. Between the plates is a gas. Particles passing through will ionize the gas just like the TPC. Because of the resistive glass plates it is possible to have a high electric field without too big avalanches. The TOF is placed around the TPC and its main goal is to identify particles with a p_t between 0.5 GeV/c and 2.5 GeV/c[17]. Particles like pions, kaons

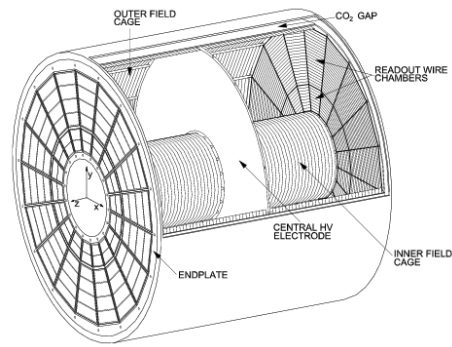


Figure 3.3 – Schematic overview of the time of flight chamber.[10]

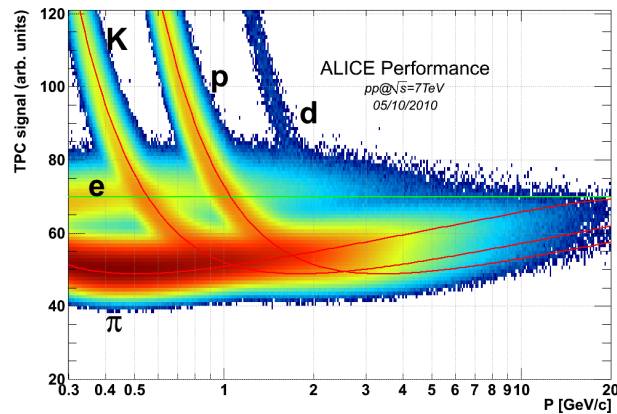


Figure 3.4 – Energy loss in the TPC for different particles. The signal is used for identification of particles[15].

and electrons are within this range. The TOF measures the time it takes for a particle to travel from the primary vertex to the detector. With the time it takes to reach the detector combined with the momentum of the particles, the mass of the particle can be calculated. The HMPID is another detector which main goal is to identify particles. The p_t -range of the HMPID is from 2.5 GeV/ c and up[18].

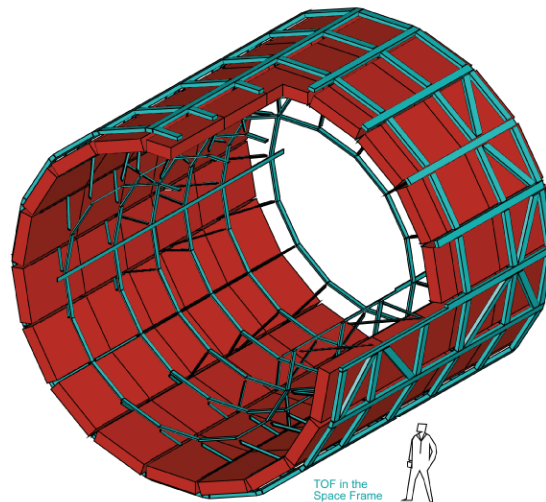


Figure 3.5 – Schematic overview of the Time of Flight detector[16].

3.2 Analysis method

3.2.1 Simulation program PYTHIA

PYTHIA[19] is an event generator for collisions of high energy particles, which was used for this research project. PYTHIA is a Monte Carlo simulation program and is based on a Monte Carlo algorithm. PYTHIA is capable of generating events between two colliding or other elementary particles. It is not possible with PYTHIA to generate Pb-Pb collisions or other collisions of non elementary particles. To gain reliable results for Pb-Pb collisions, corrections are needed. In section 6.1 are the corrections used in this research project discussed. The database PYTHIA uses contains theory and models for a number of physics aspects, including hard and soft interactions, parton distributions, initial- and final-state parton showers, multiparton interactions, fragmentation and decay. Properties of particles, such as decay modes, can be modified to optimize the simulation process for specific goals. Every particle that has been produced in an event is saved and labelled. Therefore, it is possible to see for every particle where it comes from and in which particles it has decayed. The setting used for the simulation are described in section 4.1.1.

3.2.2 ROOT

All data analysis in this research project are done within the ROOT framework. ROOT is an object-oriented program which is originally designed for particle physics data analysis and contains several features specific to this field. It is written in C++.

Chapter 4

Analysis

4.1 Simulation

The simulation procedure is described in this section. In the first part of this section is described what configurations are used for the minimum bias and the heavy flavour forced simulation. In the second part is discussed how the two types of simulation differ from each other. In the third part some general results of the D^* meson are presented.

4.1.1 Configuration

All the simulated events are p-p collisions with a center-of-mass energy $\sqrt{s} = 14$ TeV.

Only the events generated where a D^* meson is produced will be useful. To gain an efficiency as high as possible, in most of the cases we will force a $c\bar{c}$ every event. This means that with every event at least one charm anti-charm pair will be produced to boost the D^* meson production.

HardQCD : hardccbar = on

$D^{*+} \rightarrow K^- + 2\pi^+$ is the decay mode we will be interested in most of the time. To force the decay into this specific mode the following lines are included:

413 : *oneChannel =1 1 0 2 1 1 4 2 1*
421 : *oneChannel =1 1 0 2 1 1 - 3 2 1*

The first line states that every D^{*+} meson is forced into a D^0 and a π^+ when decaying. The second line states that every D^0 meson decays following $D^0 \rightarrow K^- + \pi^+$. These settings suffice for both the particles and the anti-particles.

To correct the bias gained by forcing decay modes and charm quarks, the same simulation is ran with minimum bias settings. Correction factors will be calculated in the next section by comparing the forced simulation with the realistic minimum bias simulation. For the minimum bias simulation the following lines are used:

SoftQCD : inelastic =on
SoftQCD : centralDiffractive =off

4.1.2 Comparison heavy flavour forced and minimum bias simulation

In this section, the results of the heavy flavour (HF) forced simulation is compared to that of the minimum bias. The PYTHIA simulation with the heavy flavour forced configuration produces a lot more D^* mesons than in minimum bias configuration. This is

due to the fact that a charm anti-charm quark pair is produced every collision. However, the production of D^* mesons has two components: the prompt and the feed-down component. Prompt D^* mesons are produced when a c and a \bar{d} -quark form a meson together. Feed-down D^* mesons are produced when for example a B meson decays into a D^* meson. This second component, however, will not be enhanced by the HF forced configuration. For a realistic outcome both of the components should be enhanced equally. Therefore, the enhancement of the number of D^* mesons should be the same factor in all the transverse momentum (p_T) regions. The results of both the HF forced configuration as well as the minimum bias simulation are shown in figure 4.1.

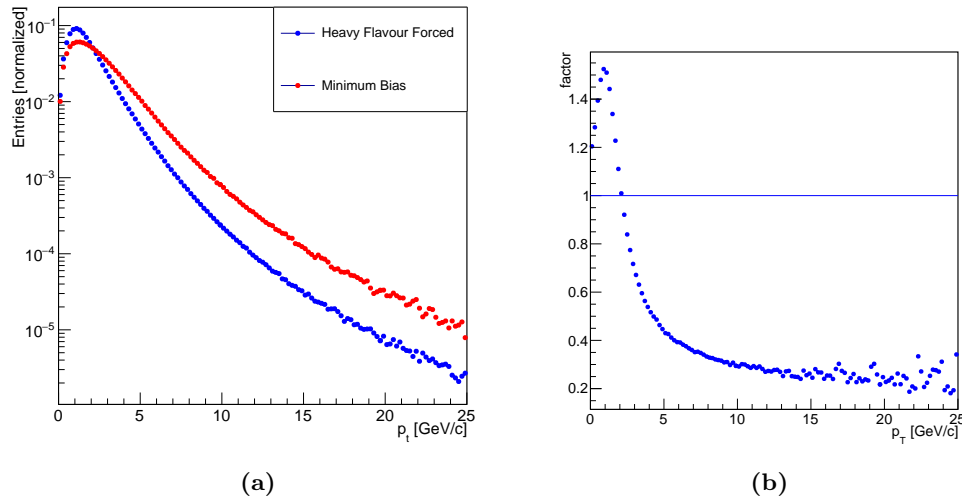


Figure 4.1 – The normalized p_t -distribution of the D^* meson is shown in 4.1a and the factor per p_t bin is shown in 4.1b. The graph shows that not all the p_t regions are enhanced by the same factor. The results of the HF forced simulation will be corrected by the values shown in 4.1b

Figure 4.1a shows that the distribution of the simulations with the HF forced settings is shifted compared to the distribution obtained from the simulation with minimum bias configuration. Results from the HF forced settings will therefore be corrected by the values presented in figure p_T region.

Forcing a charm anti-charm pair every event is not the only configuration which can give a bias in the results of the simulation. Forcing the D^* meson and the D^0 meson in only one decay channel can also give a bias in the outcome. A systematic error can be produced by the fact that a decay is not independent of the mother particle. This would mean that the branching ratio of a decay is dependent of the p_t of the motherparticle and will lead to another possible bias in the p_t distribution of D mesons. To have a good insight in this bias and in the difference of the p_t distribution between a forced and a normal sample, a normalized p_t distribution of D^0 mesons is shown in 4.2 for minimum bias and setting with all D^* mesons forced into the $D^{*+} \rightarrow D^0 + \pi^+$ decay mode. Because the figure shows no significant difference between the two settings, no correction will be used for using this setting.

4.1.3 General characteristics D^* meson production

In order to study the difference in performance of the D^* meson reconstruction after the ITS upgrade in context first will be looked at the general characteristics of the D^* meson. This study will focus on the direction in which the D^* mesons go after the collision, the way D^* mesons decay into their decay products and how the D^0 meson decays after it is produced. For the decay of the D^* meson will be looked at all three decays, but for the D^0 meson will only looked at the decay modes which are hadronic and with a branching

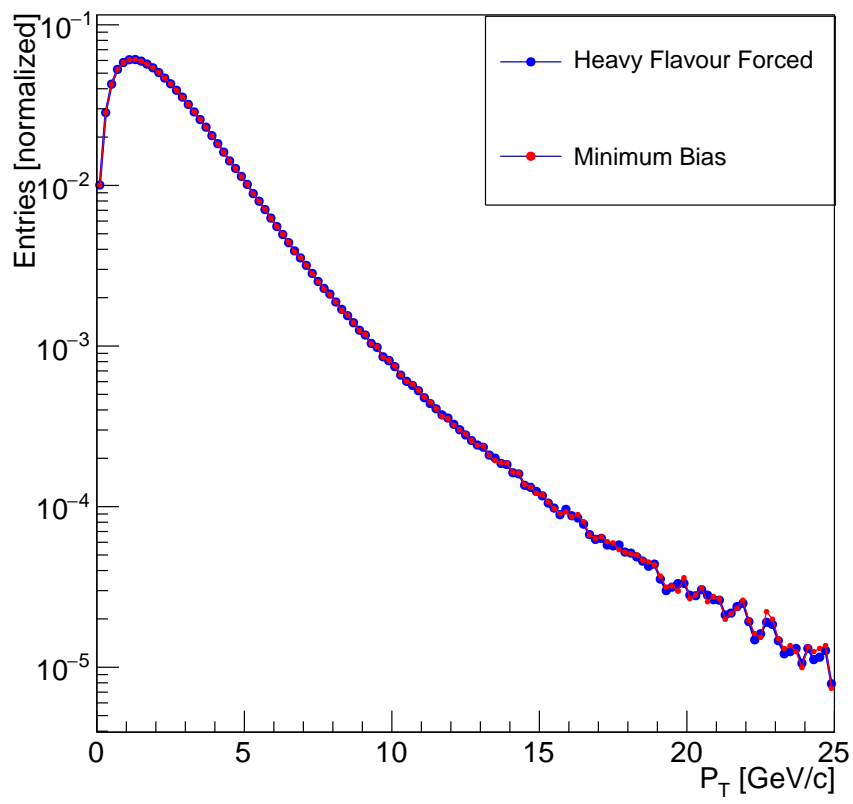


Figure 4.2 – Difference between the p_t - distribution of D^0 mesons when all D^* mesons are forced into D^0 and D^0 - mesons in minimum bias settings.

ratio higher than 2%. A hadronic decay means that all the decay products are hadrons and that therefore no electron or neutrino is created, which are difficult to detect.

To detect the particles created after a collision they must fly into the detector. As said in section (ALICE detectors) the ITS is placed completely around the collision beam. Therefore it has full acceptance in the azimuthal direction (ϕ). In terms of pseudorapidity the ITS can detect in the range of $|\eta| < 0.9$.

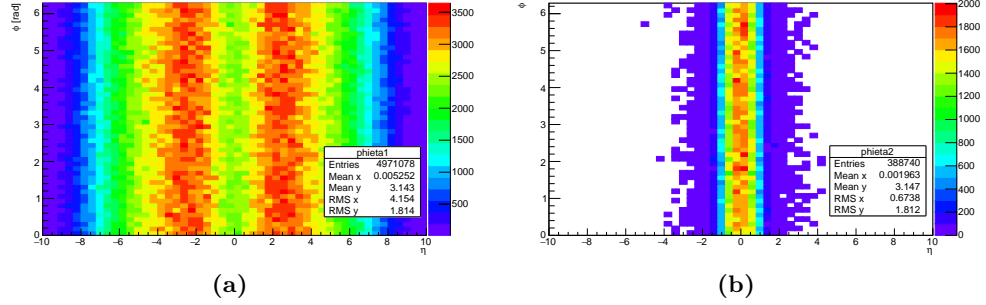


Figure 4.3 – The direction of produced D^* mesons in the $\eta\phi$ - plane. The pseudorapidity is plotted on the x-axis and the azimuthal angle ϕ is plotted on the y-axis. Left figure shows all produced D^* mesons. The right figure shows only the D^* mesons within the η - acceptance of the ALICE detectors.

Figure 4.3 shows in which direction the produced D^* mesons travel in the $\phi\eta$ -plane. In figure 4.3a all the produced D^* mesons are shown and in figure 4.3b the directions are shown of the D^* mesons with decay products within the η -range of the detector. Figure 4.3a shows that most of the D^* mesons produced, travel with a pseudorapidity of $2 < |\eta| < 4$. This is understandable from the kinematics of the collision and the acceleration of the protons before colliding. The higher the acceleration of the proton particles, the higher the momentum of produced particles will be, so the higher $|\eta|$ becomes. The ITS detector has a range of $|\eta| < 0.9$. This means that a part of the D^* mesons cannot be detected because they remain outside the range of the detector. Of the roughly 5 million D^* mesons produced in total only 0.39 million D^* mesons can be detected due to direction in which the decay products of the D^* particles travel. Figure 4.3b shows that there are also D^* mesons which can be detected while they travel out of range of the detector. This is possible due to the fact that their decay products are all inside the range of the detector.

Before the D^* mesons reach the detector they decay into decay products before reaching an ALICE detector. D^* mesons have three known possible decay channels:

$$\begin{aligned}
 D^{*+} &\rightarrow D^0 + \pi^+ && (67.7\% \pm 0.5) \\
 D^{*+} &\rightarrow D^+ + \pi^0 && (30.7\% \pm 0.5) \\
 D^{*+} &\rightarrow D^+ + \gamma && (1.6\% \pm 0.4)
 \end{aligned}$$

When reconstructing the D^* from its decay products the first decay channel is used the most. In figure 4.4 this decay channel is shown in red.

When the D^* is decayed into the a D^0 and a π^+ . The π^+ does not decay any further and goes straight into the detector. The D^0 however does decay before it will enter the detector. The D^0 can decay in a lot of different modes. These decay modes can be divided in hadronic decay modes and leptonic decay modes. In leptonic decay modes are most of the time electrons and neutrinos produced with other decay particles. These produced neutrinos and electrons are much harder to reconstruct than hadrons. In this thesis the focus will therefore be on the hadronic decay modes where no leptons are produced. In figure 4.5 are the hadronic decay modes shown with a branching ratio higher than 2%. This means that only the decay modes with a likelihood of higher than 2% are shown.

In figure 4.5 is the red line the D^0 particles which come from the D^* for the different p_t -regions and therefore the same line as the red line in figure 4.5. The second line is the

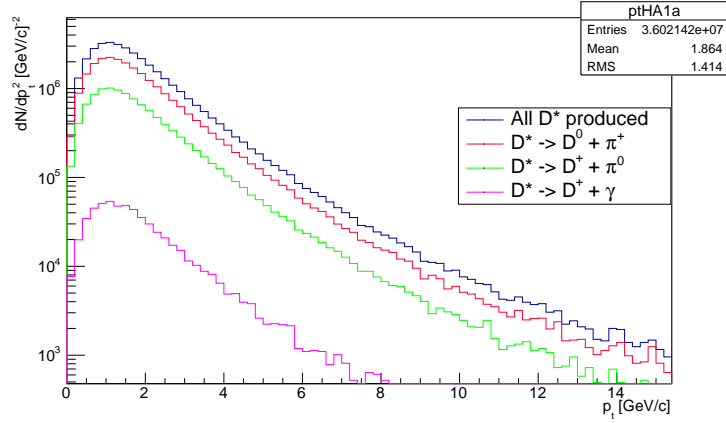


Figure 4.4 – The p_t - distribution of the D^* meson. Blue is the p_t - distribution of all produced D^* mesons. Red is are the D^* mesons decayed into a D^0 . Pink and green are p_t -distributions of D^* decaying into a D^+ . HF forced settings are used. Decay modes are not forced

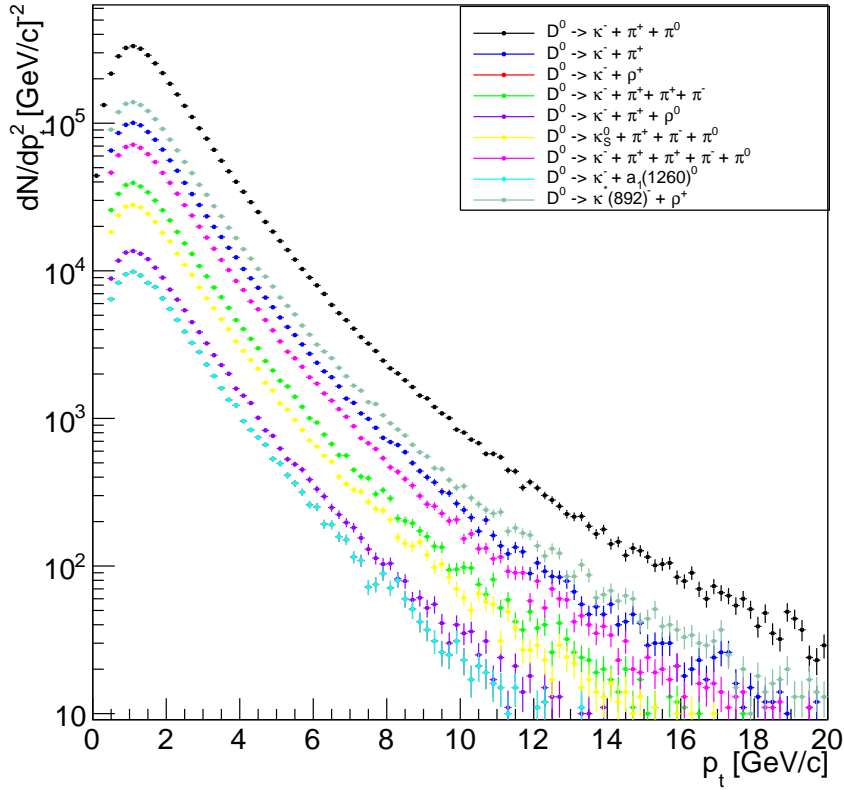


Figure 4.5 – The p_t - distribution of D^0 mesons decaying through different modes. In blue the p_t - distribution of the D^0 mesons decaying into $K\pi^+$ is shown. These particles are used for reconstruction. HF forced settings are used. Decay modes are not forced

number D^0 particles decayed by the specified mode. The decay mode $D^* \rightarrow K + 2\pi^+$ which is investigated in this thesis is shown in the upper-left graph. For comparison of the different decay modes can be looked at figure 4.5. The graph shows that the $D^0 \rightarrow K + \pi^+$ is not the decay mode where the most D^0 particles decay in. There are however other

factors which play a role for a good decay mode. The $D^0 \rightarrow K + \pi^+ + \pi^0$ for example, has better statistics but also produces an extra pion. As described in section 4.2.1 this extra π^0 will produce a lot more background and will result in a lower significance. This is the reason why there is chosen for the de decay mode without the π^0 . By the decay mode of the $D^0 \rightarrow K^*(892)^- + \rho^+$ should be mentioned that the $K^*(892)^+$ will decay further before reaching the detector. This is the reason why $D^0 \rightarrow K^- + \pi^+$ is chosen best to investigate the D*-meson.

The part of the produced D* mesons that can be detected an reconstructed is called the acceptance. To calculate the acceptance, the total number of D* mesons produced is divided by the D* mesons which daughter particles are all in the η -region of $|\eta| < 0.9$ and have a p_t of more than 40 MeV/c. The acceptance of D* mesons decayed following $D^{*+} \rightarrow K^- + 2\pi^+$ are plotted in figure 4.6. The difference is shown between the acceptance the acceptance before and after the upgrade of the ITS.

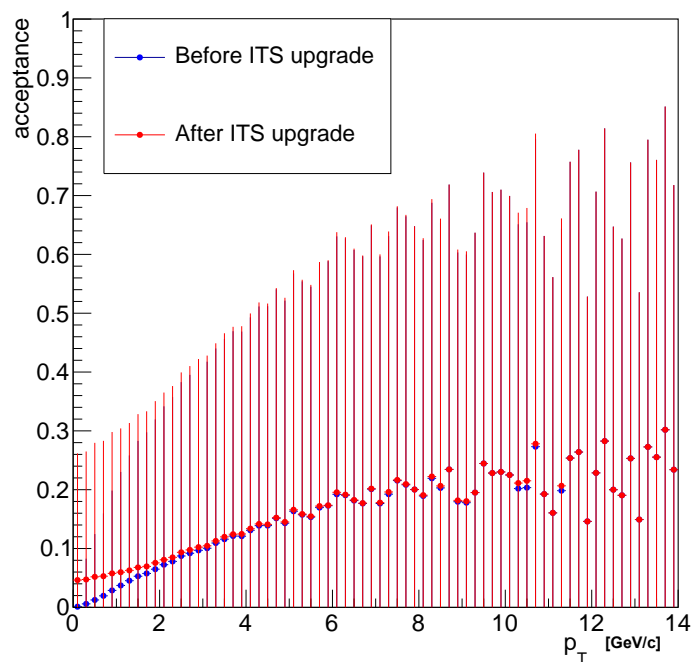


Figure 4.6 – Acceptance of D* mesons decaying into $K^- \pi^+ \pi^+$ through the D^0 meson

4.2 Real data

Real data, unlike data from simulations, is not only obtained by a signal. The data is, in real life, distorted by background. The significance of a measurement is determent the following:

$$significance = \frac{S}{\sqrt{S + B}}.$$

S is the part of the data which originates from the signal and B is the part which originates from background. When detecting particles with detectors, the background is produced due to the finite resolution of these detectors. Because of that finite resolution, the position and the p_t of a particle cannot be measured exactly. This uncertainty makes reconstructing particles more difficult. Especially reconstructing particles with multiple decay points, such as the D* meson. The two main factors producing background are an error in the direct measurement of properties of a particle, such as momentum and energy, and the difficulty to reconstruct all particles after decaying.

4.2.1 Invariant Mass method

To reconstruct the D^* mesons, the invariant mass method was used. Because D^* mesons have such a short lifetime, they decay before they reach the detector. Therefore it is not possible to measure them directly. Even the D^0 mesons have decayed before they reach the detector. The only particles detected are the K^- and the two π^+ particles where the D^* meson has decayed into via $D^* \rightarrow D^0 + \pi^+ \rightarrow K^- + 2\pi^+$. The invariant mass is a quantity that is conserved throughout the process of decaying. The invariant mass of the K^- and the two π^+ particles together is the same as the invariant mass of the D^* meson. The invariant mass of a particle can be obtained from its energy and momentum and is given by the following equation:

$$Mc^2 = \sqrt{E^2 - (pc)^2}$$

Writing this in natural units with $c=1$ this becomes

$$M = \sqrt{E^2 - p^2}$$

Where M is the invariant mass of a particle, E the total energy and p the momentum of the particle. Here, E is defined as $E = \sqrt{m^2 + p^2}$ in natural units. To calculate the invariant mass of the D^* mesons via the decay products K^- and π^+ , the following formula is applicable:

$$M_{D^*} = \sqrt{(E_{\pi_1^+} + E_{\pi_2^+} + E_{K^-})^2 - (p_{\pi_1^+} + p_{\pi_2^+} + p_{K^-})^2}$$

The invariant mass of the D^* meson can now be calculated. However, a lot of π^+ and K^- particles are produced after a collision, and only a small part of the K^- and the π^+ particles produced, come from a D^* mesons. When combining a K^- and two π^+ particles which do not come from the same D^* a random value for the invariant mass is produced and will therefore contribute to the background. When no selections are made which kaons with which pions may be combined, the background is so high that they D^* mesons cannot be distinguished from the background. To reduce background and get a clearer view of the invariant mass of the D^* meson cuts can be performed (this will be discussed in the next section). Another way to reduce background is to calculate the difference between the invariant mass of the D^* mesons and the invariant mass of the D^0 mesons. When subtracting the invariant mass of the D^* mesons by the invariant mass of the D^0 mesons, a lot of background from the D^0 mesons will vanish without losing much signal. Therefore, the invariant mass plots will be shown as the difference between D^* and D^0 mesons.

4.2.2 Performed cuts

Another method to reduce the background is to reject the particles that come from other decays. Selecting the particles which do not contribute to the signal can be done by looking at topological characteristics of the π^+ and K^- particles. This principle will be further explained by two examples. First, the topological cut based on the combined flight lines of the decay particles, and second the topological cut based on the product of impact parameters.

As discussed in chapter 3.1.1, the primary and secondary vertex of the D^* meson can be reconstructed by the ITS detector. The primary vertex is the place where the D^* meson is produced and the secondary vertex is the position where the D^* meson decays into the D^0 and the π^+ particles. With this information, the flight line of the D^* meson can be determined. In reality, the lifetime of the D^* meson is so short that they cannot be distinguished from each other. The primary and secondary vertex of the D^0 however, can be reconstructed and distinguished. When the track of the D^0 particle is known, it can be extrapolated after the decay point. With this information, it can be checked if the direction of the π^+ and K^- particles together correspond with the track of a D^0

meson. With the direction of the decay particles and the direction of the D^0 meson the angle θ can be calculated as shown in figure 4.7. Based on this value a π^+K^- -couple can be rejected as a decay product of a D^0 meson. Another cut that can be used is

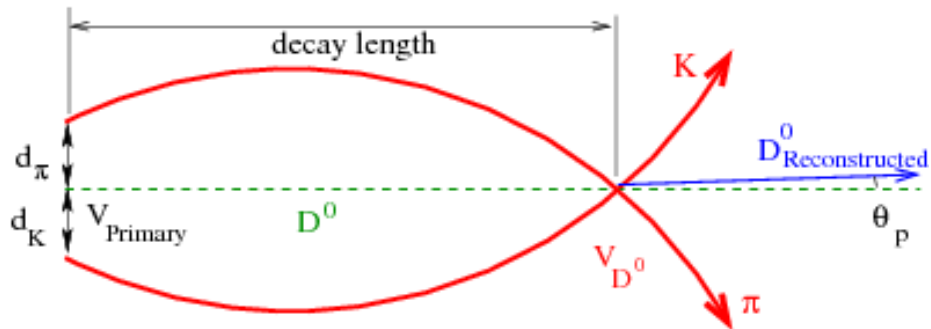


Figure 4.7 – Schematic overview of a D^0 decay [21]

based on the product of the impact parameters of the K^- and the π^+ particles coming from the D^0 meson. The impact parameter is the extrapolated distance between an incoming particle's path and a scattering center. This product of two impact parameters is symmetric when two random particles are created. However, when the K^- and the π^+ particles come from the D^0 meson this is not the case. The K^- particle has more mass than the π^+ particle and will therefore be less bent by the magnetic field in the detector. This will give the asymmetric product. Therefore, particles with a symmetric impact parameter product can also be rejected to lower the background.

Before reconstructing the D^* meson and performing cuts to lower the background, candidates are defined. Candidates are particles with enough hits in different detectors to reconstruct the particles with enough precision. The first requirement is that a particle has at least two hits in the ITS detector with at least one hit in one of the first two layers. In the TPC are 70 associated space points required. A more detailed description of the selection requirements can be found here[1]. The cut parameters described are also used.

Chapter 5

Results p_t -range

When the ITS detector is upgraded in 2020, the detector will have an extra silicon layer, but also the distance between the collision point and the first silicon layer becomes smaller. The minimum transverse momentum of a particle to be detected with a sufficient resolution will decrease due to these upgrades. The minimum transverse momentum will change from 100MeV, which is now necessary for a good measurement, to 40 MeV. When investigating what percentage of D^* mesons with low p_t can be detected, the decay particle with the lowest transverse momentum will have a p_t lower than 40 MeV/c more often than other decay particles. In the decay $D^{*+} \rightarrow D^0 + \pi^+ \rightarrow K^- + 2\pi^+$ the π^+ particle coming from the D^* meson will have a lower p_t than the K and the other π^+ particle. The low transverse momentum of this π^+ particle is due to the high mass of the D^0 meson in comparison with the π^+ particle. Therefore most of the momentum of the D^* meson will go to the D^0 meson when decaying this π^+ particle often referred to as *soft pion*, due to its low p_t .

The relation between the momentum of the D^* meson and the momentum of the soft pion is shown in figure 5.1. The graph shows that there is clear linear relation between the transverse momenta of the particles. The red line shows the current minimum p_t of a particle to be detected, and the green line is the new minimum p_t after the upgrade (for example 40 and 100 MeV/c). The figure shows that D^* mesons with a p_t in the range of [0,0.5] and [0.5,1] GeV/c, with the present ITS cannot be reconstructed, because of the low momentum of the soft pion. After the upgrade however, these D^* mesons can be reconstructed.

p_t range D^* (GeV/c)	p_t soft pion (GeV/c)
0 - 0.5	0.043 ± 0.016
0.5 - 1	0.067 ± 0.022
1 - 2	0.11 ± 0.03
2 - 3	0.18 ± 0.04
3 - 4	0.25 ± 0.05
4 - 5	0.3 ± 0.06
5 - 6	0.39 ± 0.07
6 - 7	0.47 ± 0.08
7 - 8	0.54 ± 0.09
8 - 10	0.64 ± 0.11
10 - 12	0.79 ± 0.13
12 - 16	0.98 ± 0.18
16 - 24	1.4 ± 0.3
24 - 36	1.9 ± 0.4
36 - 45	3.0 ± 0.6
45 - 60	3.7 ± 0.8

Table 5.1 – Corresponding values shown in figure 5.1

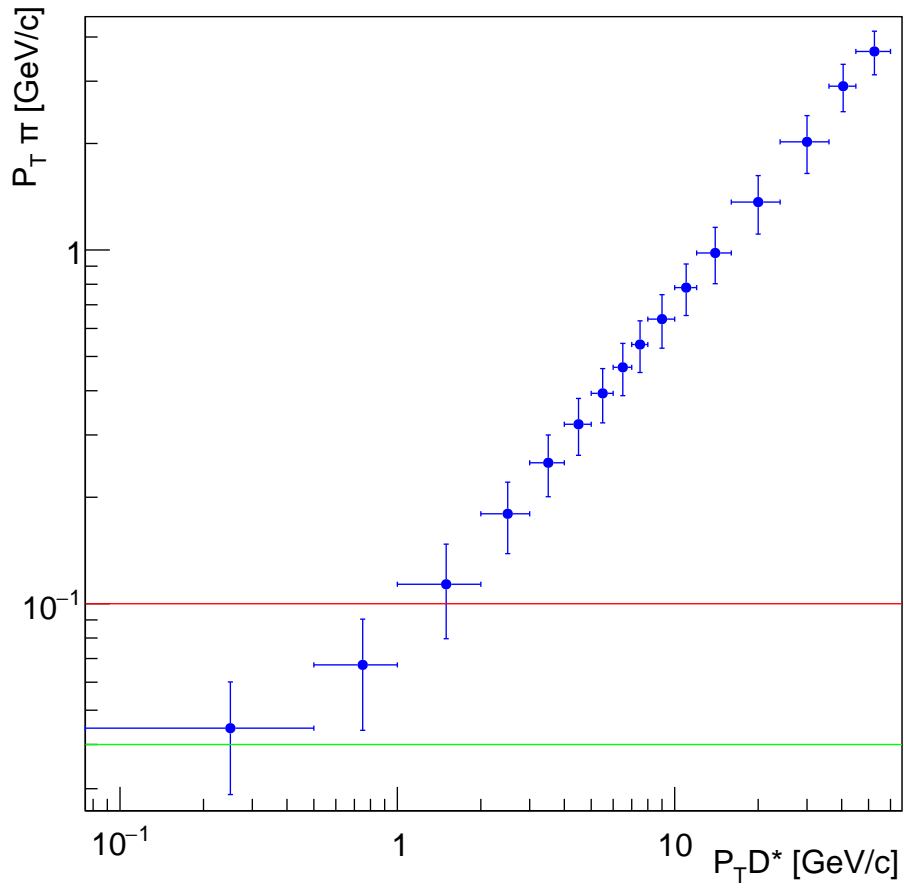


Figure 5.1 – Relation between the p_t of D^* mesons and the p_t of the corresponding soft pion. The red line indicates the present minimum p_t of a particle to be detected and is placed at 100 MeV/c. The green line indicates the minimum p_t of a particle after the upgrade of the ITS.

For the first four p_t range of the D^* meson the p_t distribution of the soft pion is shown in figure 5.2. The red line indicates 100 MeV/c and the green line indicates 40 MeV/c.

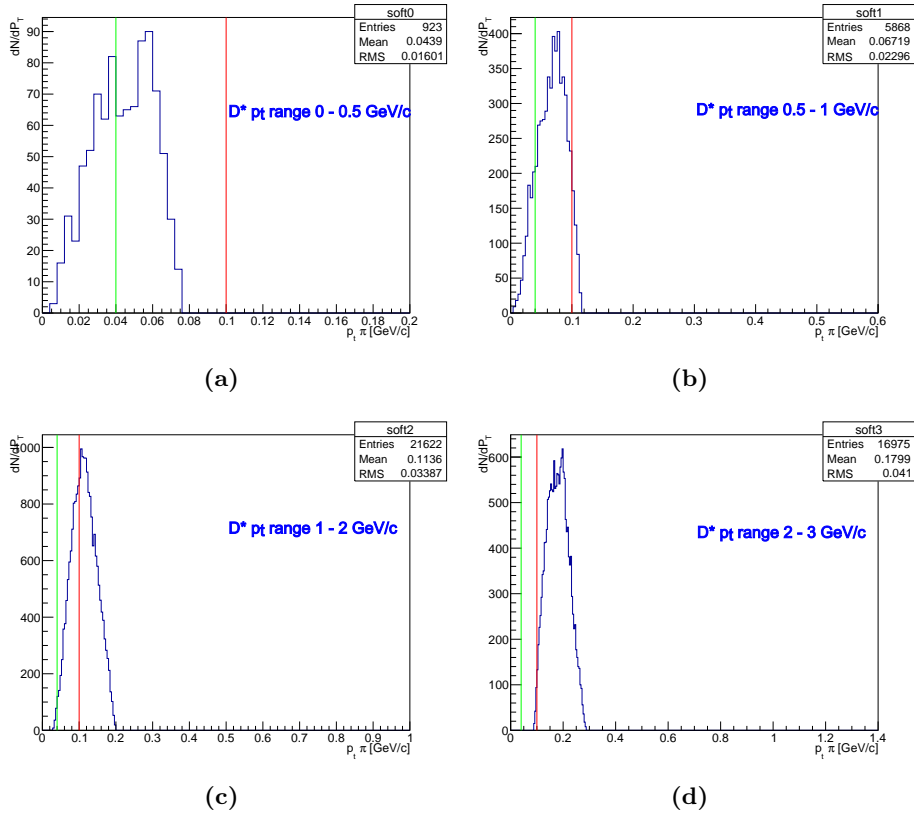


Figure 5.2 – The p_t - distribution of the soft pion for the four lowest p_t - regions shown in figure 5.1

p_t range D* (GeV/c)	minimum p_t soft pion (GeV/c)	mean p_t soft pion (GeV/c)	max p_t soft pion (GeV/c)	percentage soft pion above 40MeV/c	percentage soft pion above 100 MeV/c
0.0 - 0.5	0.008	0.044	0.076	58.2	0.0
0.5 - 1.0	0.008	0.067	0.116	89.1	11.0
1.0 - 2.0	0.032	0.114	0.200	99.4	63.
2.0 - 3.0	0.092	0.180	0.288	100.0	99.7
3.0 - 4.0	0.148	0.250	0.376	100	100
4.0 - 5.0	0.204	0.322	0.468		
5.0 - 6.0	0.260	0.391	0.556		
6.0 - 7.0	0.312	0.465	0.640		
7.0 - 8.0	0.368	0.537	0.736		
8.0 - 10	0.424	0.639	0.912		
10 - 12	0.532	0.790	1.084		
12 - 16	0.640	0.977	1.420		
16 - 24	0.908	1.387	1.960		
24 - 36	1.316	1.882	2.768		
36 - 45	2.108	2.979	3.62		
45 - 60	2.88	3.705	4.54		

Table 5.2 – Corresponding values of the data shown in figure 5.2 and 5.1

Chapter 6

Results significance D*

6.1 Expected yield

Figure 6.1 shows the D* yield per event. All the D* meson with decay particles in the range of $|\eta| < 0.9$, and with a higher p_t than 0.4 MeV/c are taken into account. The total yield per region is divided by 60 million, the total number of events simulated. The blue graph shows the D* meson per event before scaling down to the minimum bias. The red graph shows the yield per event of D* mesons scaled down to minimum bias. The minimum bias simulation didn't produce any D* mesons in the last region. Therefore the scale factor of the region [36,45] GeV/c is used for the last region. The efficiency of cuts is not yet taken into account.

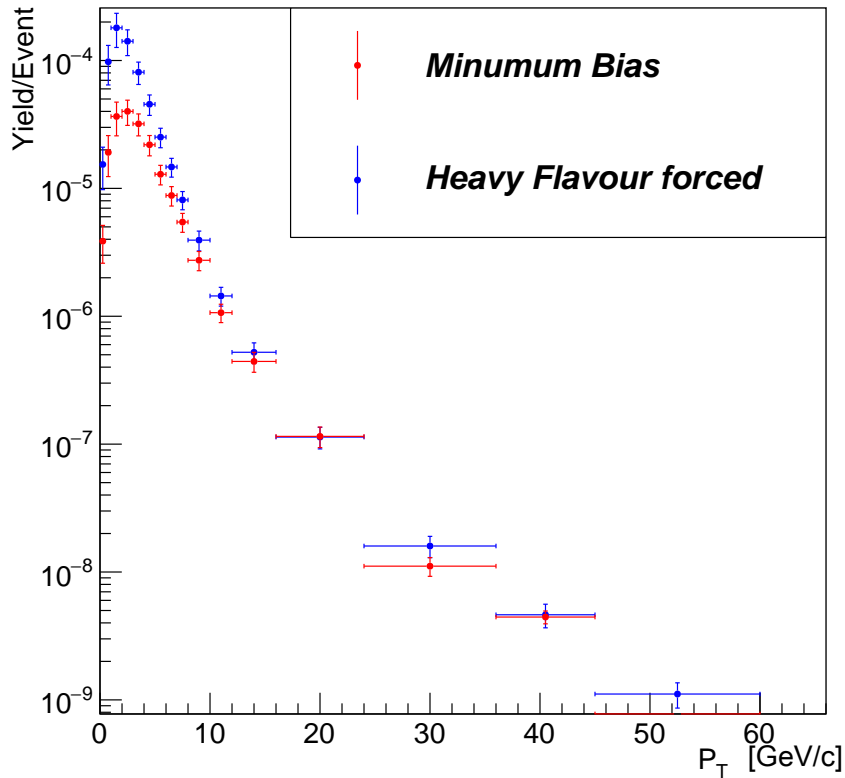


Figure 6.1 – The D* yield per event for different p_t - regions. In red for the minimum bias settings. In blue for HF forced settings.

p_t range D* (GeV/c)	yield per event minimum bias ($\times 10^{-4}$)	yield per event forced ($\times 10^{-4}$)
0.0 - 0.5	0.15 ± 0.06	0.039 ± 0.013
0.5 - 1.0	1.0 ± 0.3	0.19 ± 0.07
1.0 - 2.0	1.80 ± 0.51	0.37 ± 0.11
2.0 - 3.0	1.4 ± 0.3	0.40 ± 0.09
3.0 - 4.0	0.81 ± 0.16	0.32 ± 0.06
4.0 - 5.0	0.45 ± 0.08	0.22 ± 0.04
5.0 - 6.0	0.25 ± 0.04	0.129 ± 0.022
6.0 - 7.0	0.147 ± 0.025	0.088 ± 0.015
7.0 - 8.0	0.081 ± 0.013	0.055 ± 0.009
8.0 - 10	0.039 ± 0.007	0.027 ± 0.005
10 - 12	0.0144 ± 0.0024	0.011 ± 0.0017
12 - 16	0.00523 ± 0.00093	0.0044 ± 0.0008
16 - 24	0.00114 ± 0.00021	0.00115 ± 0.00021
24 - 36	0.00016 ± 0.00003	0.000111 ± 0.000019
36 - 45	0.000046 ± 0.000010	0.000044 ± 0.000005
45 - 60	0.000011 ± 0.000002	0.000018 ± 0.000001

Table 6.1 – Corresponding values of the data shown in figure 6.1

Figure 6.2a shows the expected yield D* mesons. This number is obtained by multiplying the yield/event by the expected p-p collision events. After the upgrade this amount is expected to be 39.8 billion. The efficiency of reconstructing is taken into account using the efficiency published in the following article [1]. For the regions where the efficiency had to be extrapolated, the efficiency of the closest given was taken. The final efficiency values are given in table 6.2. For the lead-lead collisions showed in figure 6.2a the efficiencies used to calculate the total yield are also shown in 6.2. The expected number of events is 1.6 billion. To take into account that multiple nucleons collide every event. All events are assumed to take place with 0-10% centrality, therefore a factor of 70 nucleons per collision is used to scale up. To take the quark-gluon plasma into account, the RAA factor published by the ALICE collaboration is used (see [1]). For the high p_t regions where the RAA factor had to be extrapolated is the last known value taken. For the low p_t regions the values are chosen with the assumption that the RAA-factor is 1 at 0 p_t . The values used are shown in table 6.2.

6.2 Background

To calculate the significance, the background is used from published results. For p-p collisions a data sample of 52 million events at $\sqrt{s} = 13$ TeV is used [20]. For Pb a data sample of 25,4 million events at $\sqrt{s} = 2,76$ TeV [22]. Both backgrounds are scaled down by their number of events and up by the same procedure as the yield. The background is plotted in figure 6.3. For the proton collisions values of unknown p_t -regions are extrapolated by assigning the value of the closest known p_t -region. For the Pb-Pb collisions an exponential fit is used in the form of $f(x) = e^{p_1 + p_2 * x}$ to extrapolate. The parameters of the fit are $p_1 = 14.6 \pm 1.0$ and $p_2 = -0.55 \pm 0.17$. The drop in the background in p_t bin [4,5] GeV/c in figure 6.3a is due to the fact that this region very efficient cuts could be used.

6.3 Expected significance

The expected significance is shown in figure 6.4. Figure 6.4a and figure 6.4b are the same plots but have a different scale. Figure 6.4a is plotted in normal scale and figure 6.4b is plotted in log-scale. Both figures show that the significance of p-p collisions is

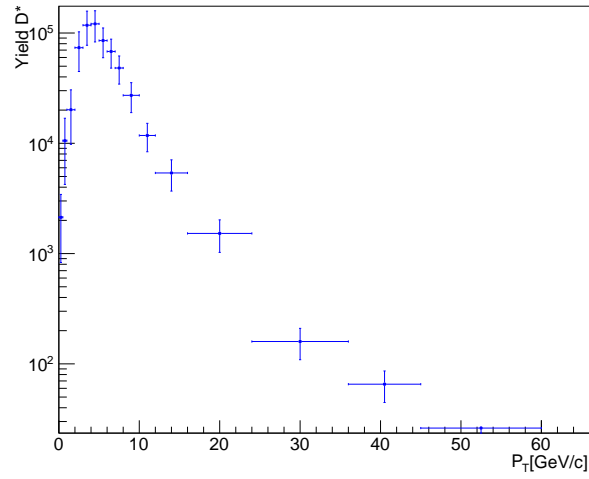
p_T range (GeV/c)	R_{AA} -factor	efficiency Pb-Pb collisions	efficiency p-p collisions
0.0 - 0.5	0.9 ± 0.1	0.0022	0.015
0.5 - 1.0	0.8 ± 0.1	0.0022	0.015
1.0 - 2.0	0.65 ± 0.1	0.0022	0.015
2.0 - 3.0	0.51 ± 0.1	0.0022	0.05
3.0 - 4.0	0.37 ± 0.06	0.009	0.1
4.0 - 5.0	0.33 ± 0.05	0.015	0.15
5.0 - 6.0	0.27 ± 0.07	0.025	0.18
6.0 - 7.0	0.28 ± 0.04	0.04	0.21
7.0 - 8.0	0.28 ± 0.04	0.04	0.24
8.0 - 10	0.26 ± 0.03	0.08	0.27
10 - 12	0.26 ± 0.03	0.08	0.30
12 - 16	0.35 ± 0.06	0.09	0.33
16 - 24	0.35 ± 0.06	0.09	0.36
24 - 36	0.35 ± 0.06	0.09	0.39
36 - 45	0.35 ± 0.06	0.09	0.40
45 - 60	0.35 ± 0.06	0.09	0.40

Table 6.2 – Values used to calculate the total yield D* mesons from the yield/event.

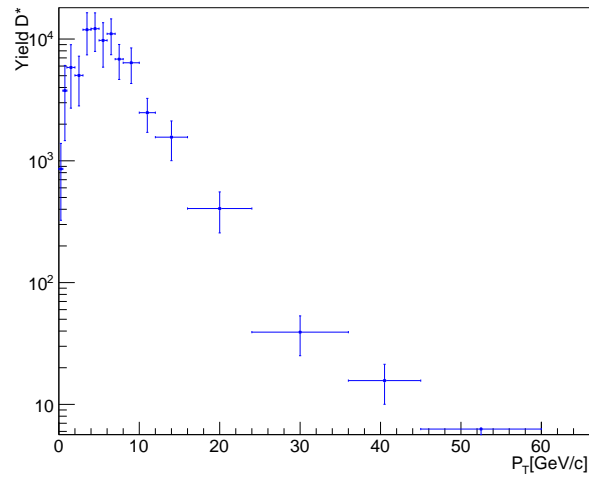
higher than 5 for all bins below 30 GeV/c. Figure 6.4b shows that the significance of p-p collisions is at lower p_t -regions significantly higher than the significance of Pb-Pb collisions. In the last two bins, however, the significance of the p-p collision drops with respect to the significance of the Pb-Pb collision. This effect is due to extrapolating the background to higher p_t -regions differently. For the p-p collision is the background assumed to be constant for the last four bins, while the background of the Pb-Pb collision drops exponentially.

p_t range D* (GeV/c)	Significance Pb-Pb collisions	Significance p-p collisions
0.0 - 0.5	0.61 ± 0.19	18 ± 6
0.5 - 1.0	3.1 ± 0.9	$71 \pm 21.$
1.0 - 2.0	5.8 ± 1.6	125 ± 32
2.0 - 3.0	6.6 ± 1.4	261 ± 51
3.0 - 4.0	20 ± 4	273 ± 47
4.0 - 5.0	27 ± 4	324 ± 51
5.0 - 6.0	28 ± 6	$194 \pm 29.$
6.0 - 7.0	40 ± 7	194 ± 29
7.0 - 8.0	33 ± 5	$175 \pm 25.$
8.0 - 10.0	43 ± 7	$128. \pm 19$
10.0 - 12.0	28 ± 4	69 ± 9.9
12.0 - 16.0	31 ± 6	62.1 ± 9.8
16.0 - 24.0	19 ± 4	$33 \pm 5.$
24.0 - 36.0	6.2 ± 1.1	6.7 ± 1.1
36.0 - 45.0	4.0 ± 0.7	2.6 ± 0.4
45.0 - 60.0	2.50 ± 0.16	1.39 ± 0.12

Table 6.3 – Corresponding values of the significance plotted in figure 6.4

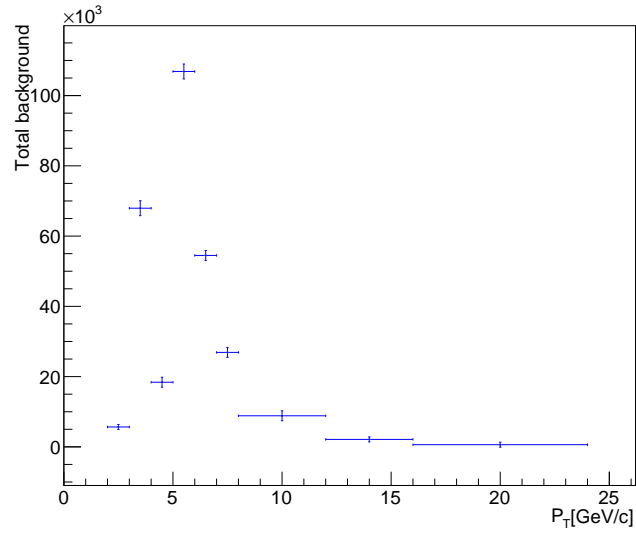


(a) Expected yield for p-p collisions

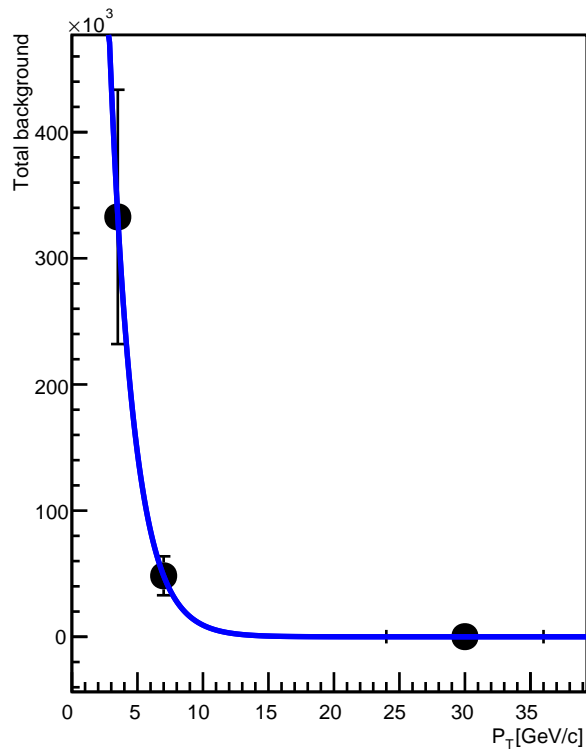


(b) Expected yield for Pb-Pb collisions

Figure 6.2 –

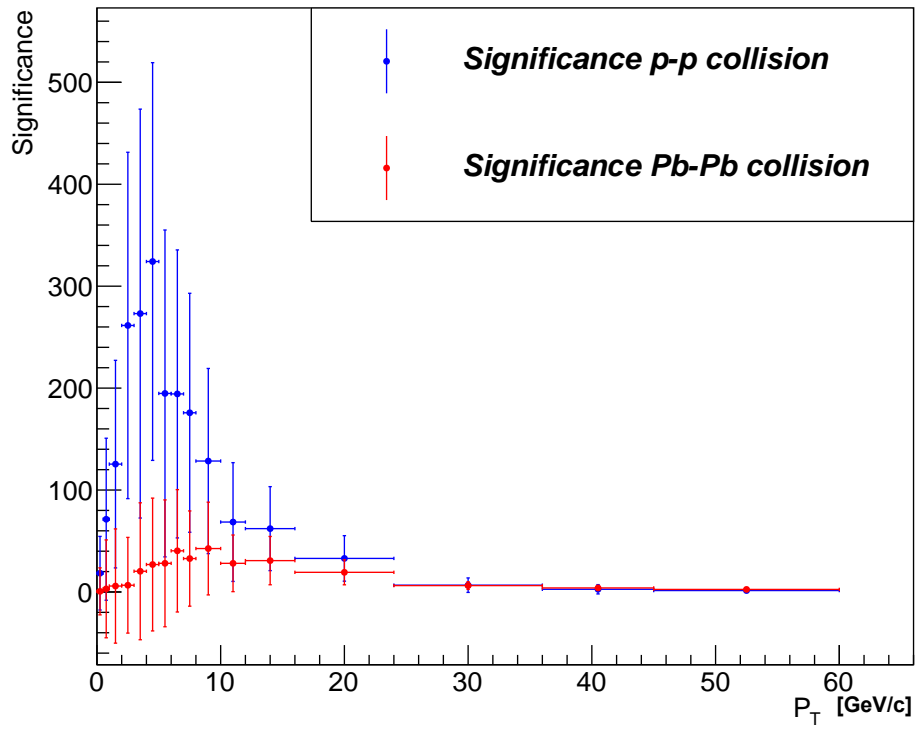


(a)

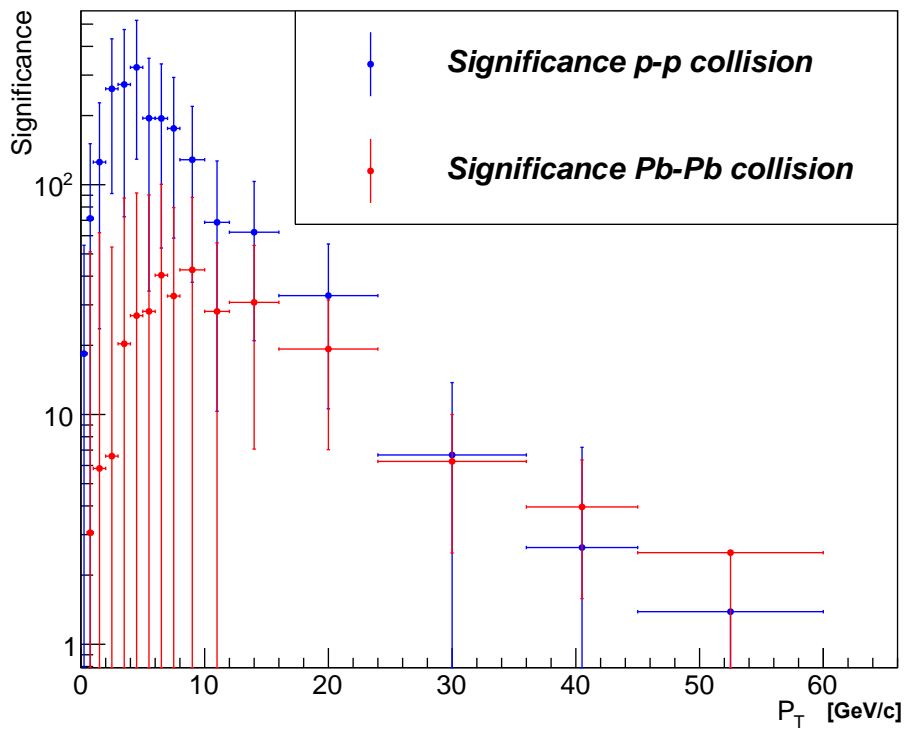


(b)

Figure 6.3 – Background used for calculated the significance shown in figure 6.4. Figure 6.3a shows the background of p-p collisions at $\sqrt{s_{NN}} = 13$ TeV. The data is taken from [20]. Figure 6.3b shows the background of Pb-Pb collisions at $\sqrt{s_{NN}} = 2.76$ TeV. The data is taken from [22]. The fit function is an exponential function with parameters 14.6 ± 1.0 and -0.55 ± 0.17 .



(a)



(b)

Figure 6.4 – Expected significance of the D^* meson produced in p - p collisions (blue) and in Pb - Pb collisions (red).

Chapter 7

Discussion

Not every part of the upgrade is taken into account, with the investigation of the performance of the ITS . As described in section 3.1.1, the two main upgrades of the ITS are an extra detector layer close to the collision point and the equipment of every layer with Silicon pixel detectors (SPD) . In this research project is the fact that particles must have a minimum p_t of 40 MeV/c instead of 100 MeV/c, to be detected by the ITS and taken into account. However, the fact that SPD's will be placed on all detector layers and will be able to detect particles with a higher resolution, is not taken into account. The higher resolution will result in more efficient cuts to reduce the background and in better reconstruction of the collision point. The background used for calculating the significance, results from p-p collisions with a center of mass energy $\sqrt{s_{NN}} = 13$ TeV and from Pb-Pb collisions at $\sqrt{s_{NN}} = 2.76$ TeV. The Yield, however, is simulated with events at $\sqrt{s_{NN}} = 14$ TeV. At present time, p-p collisions at $\sqrt{s_{NN}} = 13$ TeV and Pb-Pb collisions of $\sqrt{s_{NN}} = 5.02$ TeV take place in the LHC. This difference between energies of Pb-Pb collisions can result in more produced background. This increase in background will most probably be compensated by the better resolution of the detector layers, as better resolution of the detector would allow finer cuts.

For calculating the error in the significance only the error of the yield is taken into account. Because the error in the yield is more significant than the error in the background. However, due to extrapolating roughly in the highest three p_t regions, the error in the background is also not taken into account. Therefore, the error bars plotted in figure 6.4 should be bigger than shown.

Taken into consideration that the increase of resolution of the ITS is not taken into account, both the significance of D* meson of p-p collisions and of Pb-Pb collisions are conservative predictions. The positive effect of the better resolution is expected to be greater than the negative effect of extra background in Pb-Pb collisions.

Chapter 8

Conclusion & Outlook

8.1 Conclusion

The performance of the upgraded ITS for detecting D^* mesons has been investigated. The expected significance as well as the p_t -range in which D^* mesons can be detected after the upgrade are studied. Figure 5.2 and table 5.2 show that D^* mesons with a p_t in the region of $[0,0.5]$, $[0.5,1]$ or $[1,2]$ GeV/c can be detected significantly better than before the upgrade. At present the ITS is able to detect 63.9% of the D^* mesons in the p_t -region of $[1,2]$ GeV/c, while it can detect almost hundred percent after the upgrade. For the p_t -region $[0.5,1]$ GeV/c the percentage D^* mesons that can be detected increases from 11% to 89%. And in the p_t -region $[0,0.5]$ GeV/c the percentage is expected to increase from 0% to 58%.

The expected significance for the D^* meson is shown in figure 6.4 and table 6.3. D^* mesons produced in Pb-Pb collisions with a p_t between 1 GeV/c and 36 GeV/c have a significance higher than 5. Only D^* mesons with a p_t in the range of $[0,0.5]$ GeV/c or $[45,60]$ GeV/c have a p_t lower than 3. The maximum significance for Pb-Pb collisions is 42 and is reached in the p_t -range $[8,10]$ GeV/c. D^* mesons produced in p-p collisions with a p_t between 0 and 36 are predicted to have a significance higher than 5. D^* mesons with a p_t higher than 36 are predicted to have a significance lower than 3.

8.2 Outlook

As with every research, there are subjects which could be investigated further. In chapter 7 is discussed that the interaction between particles and the detector are not taken into account in this research project. This interaction could be further investigated using the GEANT toolkit. The difference between the performance of the ITS consisting of SPD, SDD and SSD detectors and the performance of the ITS detector containing only SPD detectors and an extra silicon layer would give a better insight in the expected significance.

Bibliography

- [1] The ALICE collaboration, 12 Oct 2012,
[arXiv:1203.2160v4](https://arxiv.org/abs/1203.2160v4) [nucl-ex]
- [2] Universität Zürich Physik-Institut, Standard Model,
<http://www.physik.uzh.ch/groups/serra/StandardModel.html>
visited at June 16,2016
- [3] Edmond Iancu, QCD in heavy ion collisions, 2 May 2012,
[arXiv:1205.0579v1](https://arxiv.org/abs/1205.0579v1) [hep-ph]
- [4] A. Grelli, Presentation Technische Universität München, 27/04/2015.
http://www.staff.science.uu.nl/~grell1101/StrongInt_TUM_Grelli_27Apr.pdf
- [5] K.A. Olive et al. (Particle Data Group), Chin. Phys. C, 38, 090001 (2014) and 2015 update
- [6] Performance of the ALICE Experiment at the CERN LHC,
<http://aliceinfo.cern.ch/ArtSubmission/node/716>
visited at June 16,2016
- [7] ALICE, A Large Ion Collider Experiment,
<http://aliceinfo.cern.ch/ITSUpgrade/>
visited at June 16,2016
- [8] P. Riedler on behalf of the ALICE collaboration.2012. Upgrade of the ALICE Detector. Physics Procedia 37 (2012) 164 – 169. *Elsevier Open Access article*
- [9] The ALICE Collaboration, K Aamodt, A Abrahantes Quintana, R Achenbach, S Acounis, D Adamová, C Adler, M Aggarwal, F Agnese, G Aglieri Rinella et al. Published 14 August 2008. Journal of Instrumentation, Volume 3, August 2008
- [10] Particle identification - Lippmann, Christian Nucl.Instrum.Meth. A666 (2012) 148-172 [arXiv:1101.3276](https://arxiv.org/abs/1101.3276) [hep-ex],
found at <https://inspirehep.net/record/884672/plots>
visited at June 16,2016
- [11] T Gunji, for the ALICE Collaboration. Future upgrade and physics perspectives of the ALICE TPC. Nuclear Physics A Volume 931, November 2014, Pages 1152–1157. QUARK MATTER 2014.
- [12] J. Alme, et al., The ALICE TPC, a large 3-dimensional tracking device with fast readout for ultra-high multiplicity events. January 12, 2010
[arXiv:1001.1950](https://arxiv.org/abs/1001.1950) [physics.ins-det]
- [13] ALICE, The ALICE Time Projection Chamber (TPC),
http://aliceinfo.cern.ch/Public/en/Chapter2/Chap2_TPC.html
visited at June 16,2016
- [14] ALICE, Time Projection Chamber,
<http://aliceinfo.cern.ch/TPC/node/7>
visited at June 16,2016

-
- [15] Charged pion identification at high pT in ALICE using TPC dE/dx - ALICE Collaboration (Bryngemark, L. for the collaboration) arXiv:1109.1896 [hep-ex], found at <https://inspirehep.net/record/927004/plots>
- [16] The ALICE Time of Flight detector,
<http://aliceinfo.cern.ch/Public/en/Chapter2/Chap2.TOF.html>
visited at June 16,2016
- [17] A. Alici, The MRPC-based ALICE Time-Of-Flight detector: status and performance.arXiv:1203.5976 [physics.ins-det]
- [18] ALICE Collaboration, The ALICE experiment at the CERN LHC.
JINST 3 (2008) S08002.
- [19] Pythia, Lund University
<http://home.thep.lu.se/~torbjorn/Pythia.html>
visited at June 16,2016
- [20] A. Veen, First look crosssection 13 TeV, presentation given at Utrecht University.
April 19, 2016.
- [21] B. S. Nilsen on behalf of the ALICE Collaboration, Heavy-flavor production in LHC pp interactions using the ALICE detector, January 25, 2014
Nucl.Phys.Proc.Suppl. 233 (2013) 201-206 arXiv:1210.7847 [hep-ex]
found at <http://inspirehep.net/record/1194115/plots>
- [22] ALICE collaboration, Transverse momentum dependence of D-meson production in Pb-Pb collisions at $\sqrt{s_{NN}}=2.76$ TeV. 14 september 2015
arXiv:1509.06888v2 [nucl-ex]

Appendix A

In this appendix, invariant mass plots of the data from LHC10f7a are shown. These invariant mass plots are not used for the calculation of the significance, but are produced before was decided to use the background discussed in section 6.2 For the data showed in figure 1, a Gaussian on top of a exponential is used as a Fit function. The exponential part of the function fits the background and the Gaussian part fits the signal.

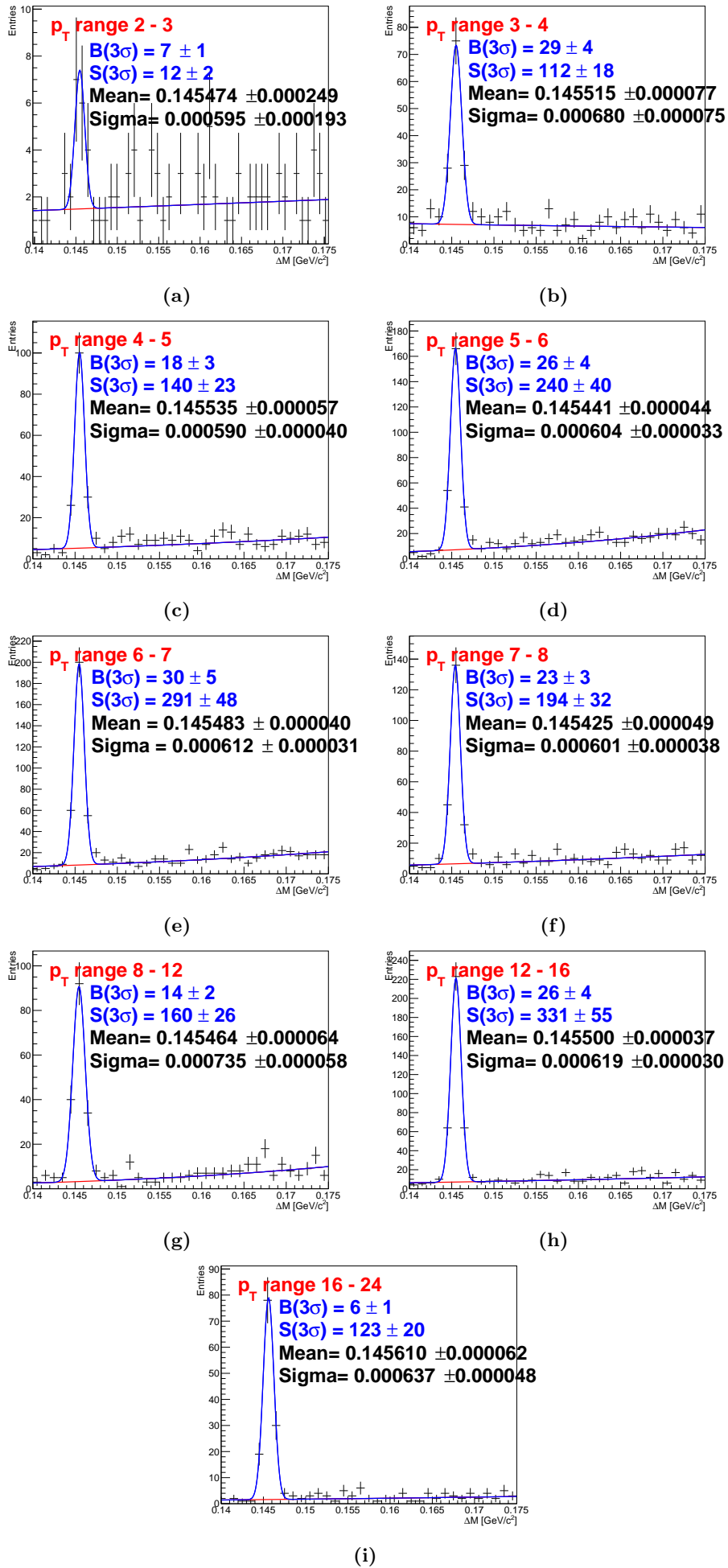


Figure 1 –